Dynamic modelling and control of an underactuated Klann-based hexapod

Edgar A. Martínez-García* and Josué Domínguez
Laboratorio de Robótica, Institute Engineering and Technology
Universidad Autónoma de Ciudad Juárez
Juárez, Mexico
edmartin@uacj.mx

Roman Lavrenov
Laboratory of Intelligent Robotics Systems, ITIS
Kazan Federal University
Kazan, Russia
lavrenov@it.kfu.ru

***Abstract*—This work discloses the dynamic control model of a hexapod robot with tripod-based walking gait. The proposed walking model is based on the Klann linkage and three main actuators to provide quasi-omnidirectional mobility. The reduced number of actuators preserve holonomy as similar as popular 18-servo hyper-redundant hexapods (three servos per leg). This work proposes two-drive differential control, one drive per lateral triplet of legs. Each triplet is synchronized in speed with different angle phase of rotation. The six limbs are synchronized with bidirectional yaw motion with the third actuator. Quasi-omnidirectional mobility was achieved and controlled by a dynamic control law that governs the robots mechanisms motion. Kinematic and dynamic results are validated through numerical simulations using a tripod gait.**

***Index Terms*—hexapod, multi-legged, Klann limb, dynamic control, underactuated mechanism, walker robot, tripod gait**

I. Introduction

Multi-legged walker robots inherently pose great locomotion capabilities due to their hype-stability over numerous complex reliefs. Some unstructured terrains include flatter, alluvial plains, farming soils, steeper, rockier uplands, watershed boundaries, drainage characterized systems and hilly terrains [1]. For human safety, multi-legged walker robots [2] are suitable to operate at dangerous landscapes where landslides, downhill creep, flows, slumps, and rock falls represent hazardous environments for humans [3]. There exist different classes of robotic hexapods developed to perform different varieties of missions and tasks that are of great utility in field applications, [12]. Multi-legged robots poses high steerage, which is essential to carry out missions in fields such as mining, forestry, construction, planetary exploration, vulcanography, search and rescue, demining, agriculture and so forth. There are few successful applications based on undearctuated limbs for walking machines such as trajectory tracking quadrupeds [15], bio-inspired hexapods [20] [14], reconfigurable stair climbing walkers [6], walking chairs [8], or similar works related to the present research [7]. Redundant walker robots such as hexapods [16] [19] require one rotary actuator per degree of freedom (DOF), which is a general complication. The joints require wider physical space, the joints mechanism require instrumentation, electrical energy consumption demand rises as the number of actuators increases [22], which drastically reduces the robot's operating time. Traditionally, multi-legged robots may require at least two actuators (2 DOF) to control one leg, one for azimuth rotation and another for elevation. In addition, incrementing the number of actuators to control a limb, the control models become redundantly kinematic. The number of independent control variables is greater in number than the DOF in the working space. Usually walker robots control is devoted for cyclod gaiting control [13], resembling biomimetic gaits [18], gaits synthesis [5], synthesis for limbs reconfiguration [4], gait planning [10] and learning [11].

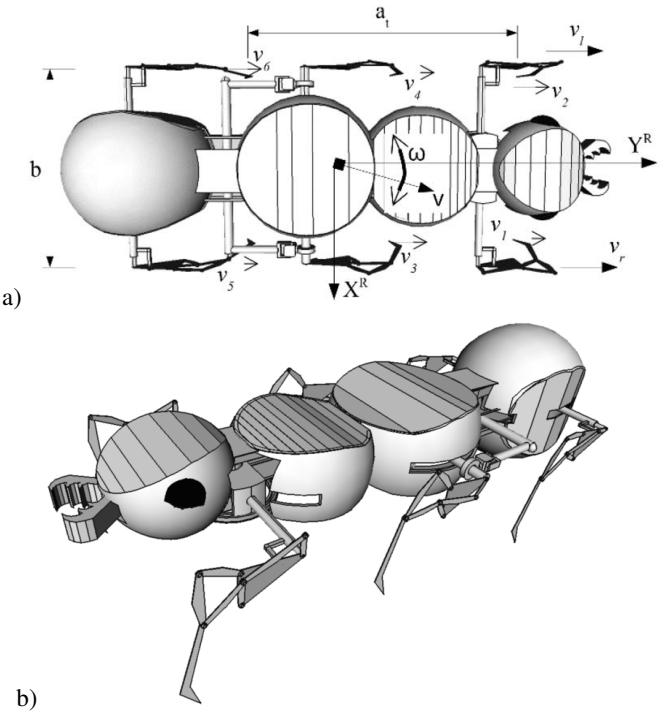

Fig. 1. Proposed quasi-omnidirectional robotic platform. a) Kinematic parameters (top view). b) Underactuated three-motor quasi-omnidirectional robot concept.

In this work's concept, an asymmetric hexapod deploying

978-1-7281-3021-7/19/$31.00 ©2019 IEEE
DOI 10.1109/DeSE.2019.00022

Klann limbs is proposed (Figure 1a). The Klann linkage is a planar mechanism with 7 passive joints, using one rotary actuator, but in this work the mechanism is also be controlled in yaw. One of our work's main contributions is the mechanical design that reduced a traditional hyoer-redundantn eighteen-servo model into an asymmetric three-motor underactuated version of hexapod, still preserving omnidirectional mobility (Figure 11b). One servomotor for limbs bidirectional synchronized steering, a second motor for driving the right-sided triplet of legs, and a third motor to drive the left-sided triplet. As a difference from other approaches [17], the proposed hexapod design is considered quasi-omnidirectional because it can reach any Cartesian point requiring a small latency time for the limbs to reach the targeted yaw. A dynamic control law is presented for the gait speed by establishing a reference torque to track a given trajectory. Each lateral triplet has the limbs position with different phase to stabilize the gait. The limbs dynamic motion model includes the kinetic and potential energy interaction model, which approaches a Euler-Lagrange solution. The presented approach provides simulations that concern the underactuated mobility space of a hexapod. In section II, the proposed underactuated mechanical design and the Klann limb kinematics are presented. In section III presentes the deduction of the dynamic control walking model and section IV provides the conclusion.

II. KLANN-BASED UNDERACTUATED KINEMATICS

The present work proposes a locomotion mechanism consisting of a differential driving system (Figure 2a), an all-limb synchronous bidirectional steering yaw mechanism (Figure 2b) and the Klann-based limbs (Figure 3). The right and left sided are differential speeds providing instantaneous velocity v_t and yileding instantaneous yaw speed, ω_t. One drive per lateral triplet of limbs, interconnected front/back sides by tracks from the central drives. The steering mechanical system of Figure 2b shows bilateral direction angle for all-limb synchronously and can turn in yaw $-\pi/4, ..., \pi/4$. The Klann mechanism (Figure 3) is an underactuated planar multi-link system, which from rotary input motion, it produces as output a cycloid trajectory (Figure 4). The links proportions are defined to optimize linear motion of the contact point at every rotary half cycle of the crank. The contact point lifts during the other rotary half cycle, before returning to the staring position. Klann [9] presented his famous invention, the "*walking device*", which is usually deployed to emulate biological limbs motion, mostly antropods. For instance, [21] developed artificial active whiskers for underwater guidance of walking robots based on the Klann mechanism. The Klann mechanism has several functional advantages as numerous advanced displacement systems have, such as stepping over obstacles, climb stairs, walking over all terrains, while not requiring a computing system to be controlled. The Klann mechanism is comprised of seven rigid links ($L_1, ..., L_7$, Figure 3a), a stretcher frame, a link used as crank handle L_1, two as seesaw that are joined to the stretcher frame (L_2 and L_5), and all of them are interconnected through pivot joints ($A, B, ..., F$). The links proportions define

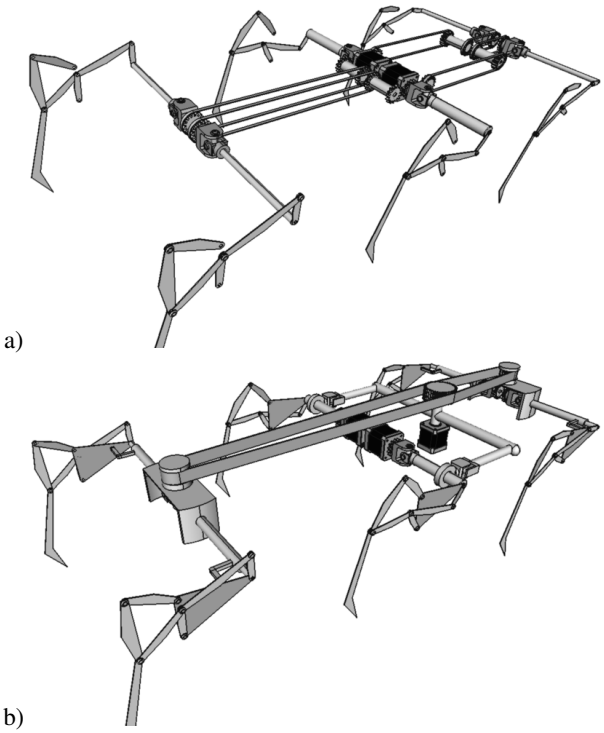

Fig. 2. Differential drive and steering mechanisms. a) driving structure. b) Lims yawing structure.

the optimize the link-foot linearity of motion with half rotation of the crank handle (Figure 3b). The rest of the crank's rotation allows that the link-foot move up to a defined height before motion return toward the staring position, repeating again the motion loop. In this work, a Klann mechanism of

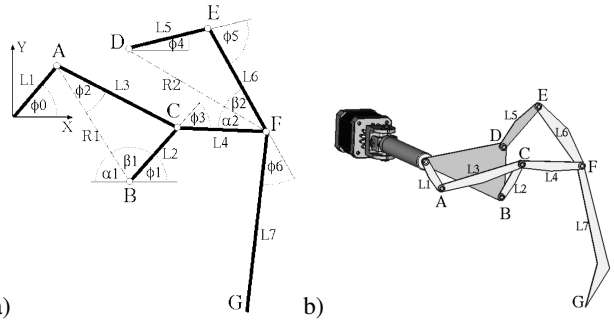

Fig. 3. Klann-based limb. a) free-body diagram. b) Klann limb with motor.

specific proportions was designed for the purpose of limbs in a tripod-like walking. The kinematic model was deduced to numerically simulate and analyze the gait tracks. The link L_1 in connection with L_3 actuate as a rotating cam with L_2 as a balancing bar. The oscillatory motion is transmitted to the coupled links L_4, L_5 and L_6 to convert the rotary motion of L_1 into linear motion in the base of the link effector L_7. Let us define the crank handle Cartesian position model of link

L_1:

$$A_x = L_1 \cos(\phi_0) \tag{1a}$$

and

$$A_y = L_1 \sin(\phi_0), \tag{1b}$$

where ϕ_0 is the motor's rotation angle conducted to the link L_1. The instantaneous distance R_1 between the passive joints A and B is calculated by

$$R_1 = \sqrt{(A_x - B_x)^2 + (A_y - B_y)^2}, \tag{2}$$

forming a non stationary angle α_1 of the straight line $\overline{AB}$ with respect to (w.r.t.) the horizontal axis, such that

$$\alpha_1 = \tan^{-1}\left(\frac{A_y - B_y}{A_x - B_x}\right), \tag{3}$$

with complementary angle β_1 that comprises the triangle $\overline{ABC}$ and is obtained through the law of Cosines:

$$\beta_1 = \cos^{-1}\left(\frac{R_1^2 + L_2^2 - L_3^2}{2R_1 L_2}\right). \tag{4}$$

Therefore, the angle ϕ_1 governs the motion of L_2 and is inferred by

$$\phi_1 = (\alpha_1 - \beta_1) - \pi. \tag{5}$$

Thus, through the angle ϕ_1, the Cartesian position of the node C is deduced by the expressions

$$C_x = B_x + L_2 \cos(\phi_1) \tag{6a}$$

and

$$C_y = B_y + L_2 \sin(\phi_1), \tag{6b}$$

where B_x and B_y describe the L_2 coordinates. By knowing the positions of nodes A and C, the angle ϕ_2 can be obtained using

$$\phi_2 = \tan^{-1}\left(\frac{C_y - A_y}{C_x - A_x}\right). \tag{7}$$

Therefore, as for the angle ϕ_3 its model is:

$$\phi_3 = \phi_2 + \Delta\phi_1, \tag{8}$$

where $\Delta\phi_1 = 160.53 \cdot \pi/180 + \pi$ being the slope angle of L_3. Thus, in order to model the position of joint F, the following expression is established where the links L_1, L_3 and L_4 are involved in describing the ϕ_2 behaviour. Thus,

$$F_x = L_1 \cos\phi_0 + L_3 \cos\phi_2 + L_4 \cos\phi_3 \tag{9a}$$

and

$$F_y = L_1 \sin\phi_0 + L_3 \sin\phi_2 + L_4 \sin\phi_3. \tag{9b}$$

Furthermore, to find the magnitude of R_2, the positions of joints D and F are used in the following expression:

$$R_2 = \sqrt{(F_x - D_x)^2 + (F_y - D_y)^2}. \tag{10}$$

Moreover, the angle α_2 is obtained w.r.t. the absolute horizontal plane by

$$\alpha_2 = \tan^{-1}\left(\frac{F_y - D_y}{F_x - D_x}\right). \tag{11}$$

It follows that, by using the segments L_5, L_6 and R_2 within the law of Cosines, the inner angle β_2 is obtined by

$$\beta_2 = \cos^{-1}\left(\frac{R_2^2 + L_6^2 - L_5^2}{2R_2 L_6}\right). \tag{12}$$

The angle ϕ_4 determines ths L_6 slope w.r.t. node F,

$$\phi_4 = (\alpha_2 - \beta_2) - \pi. \tag{13}$$

By using the links L_1, L_3, L_4 y L_6 the instantaneous position of node E is obtained,

$$E_x = L_1 \cos\phi_0 + L_3 \cos\phi_2 + L_4 \cos\phi_3 + L_6 \cos\phi_4 \tag{14a}$$

and

$$E_y = L_1 \sin\phi_0 + L_3 \sin\phi_2 + L_4 \sin\phi_3 + L_6 \sin\phi_4, \tag{14b}$$

with the coordinates of joints D and E known, the angle ϕ_5 is calculated with the expression:

$$\phi_5 = \tan^{-1}\left(\frac{E_y - D_y}{E_x - D_x}\right). \tag{15}$$

In addition, to determine the gait angular profile, the angle slope angle $\Delta\phi_2$ is included,

$$\phi_6 = \phi 4 + \Delta\phi_2, \tag{16}$$

where $\Delta\phi_2 = 90.6 \cdot \pi/180 + \pi/2$. Finally, the node G represents the Klann limb's end effector

$$G_x = L_1 \cos\phi_0 + L_3 \cos\phi_2 + L_4 \cos\phi_3 + L_7 \cos\phi_6 \tag{17a}$$

and

$$G_y = L_1 \sin\phi_0 + L_3 \sin\phi_2 + L_4 \sin\phi_3 + L_7 \sin\phi_6. \tag{17b}$$

Therefore, by computing the previous kinematic formulation, the joints $A, \ldots, F$ and limb's contact point **G** are numerically simulated as shown by Figure 4.

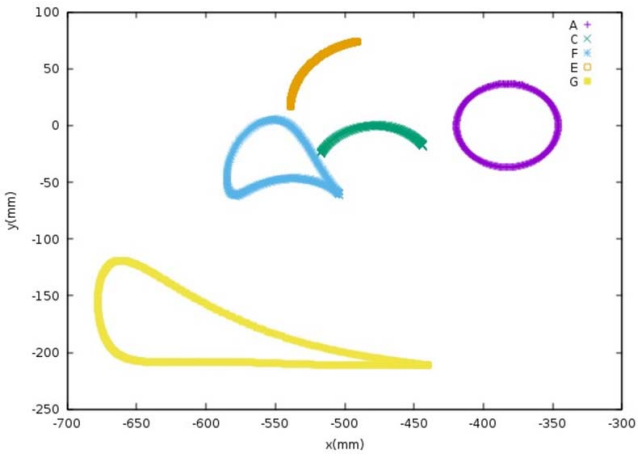

Fig. 4. Numerical simulation of the Klanns joints Cartesian motion.

III. WALKING CONTROL LAW

The equations presented here are used to infer the robot's state vector and its higher order derivatives about its locomotion overtime. The independent control joint variables are the orientation angles $\dot{\varphi}_s$, which governs the Klann rotary shaft positions. The limbs' end-effectors kinematic state vector is $\mathbf{p} = (p_x, p_y, p_z)^\top$, with $\sin(\varphi_1) \triangleq s_1, \ldots, \cos(\varphi_1+\varphi_2) \triangleq c_{12}$ and so forth, in order to simplify expressions. Thus, stating $\mathbf{p}$ by

$$\mathbf{p} = \begin{bmatrix} s_s & 0 & 0 \\ 0 & 1 & 0 \\ 0 & 0 & c_s \end{bmatrix}^\top \left[l_1 \begin{bmatrix} c_0 \\ s_0 \\ c_0 \end{bmatrix} + l_3 \begin{bmatrix} c_2 \\ s_2 \\ c_2 \end{bmatrix} + l_4 \begin{bmatrix} c_3 \\ s_3 \\ c_3 \end{bmatrix} + l_7 \begin{bmatrix} c_6 \\ s_6 \\ c_6 \end{bmatrix} \right] \tag{18}$$

Let us establish each limbs inertial frame into the robots fixed coordinate system located ideally at its geometric center

$$\mathbf{q}_i = \mathbf{R}_z \cdot \left(\frac{-\pi}{2} \right) \mathbf{p}_i + \begin{pmatrix} \Delta_x \\ \Delta_z \end{pmatrix} \tag{19}$$

There is one pair of Cartesian increments Δx and Δz for each limb defined by translation coordinates $[(\Delta x, \Delta z)$, $(\Delta x, -\Delta z)$, $(0, -\Delta z)$, $(0, \Delta z)$, $(-\Delta x, \Delta z)$, $(-\Delta x, -\Delta z)]$, w.r.t. the center of the hexapod. The Euler rotation matrix $\mathbf{R}_z$ transforms each limb i, and their end-effectors position vectors $\mathbf{p}_i$. In addition, the robots longitudinal and angular speed models described by the control vector is $\dot{\mathbf{u}} = (v, \omega)^\top$. The absolute robots velocity is modeled by the averaged lateral limb Cartesian speeds

$$v_t = \frac{v_r + v_l}{2} = \frac{\|\dot{\mathbf{q}}_{ir} + \dot{\mathbf{q}}_{il}\|}{2} = \frac{\sqrt[2]{(\dot{x}_r + \dot{x}_l)^2 + (\dot{y}_r + \dot{y}_l)^2}}{2} \tag{20}$$

where v_t is the robot's instantaneous velocity, v_r and v_l are the limbs' instantaneous lateral speeds at right and left sides respectively. The Klann limb direct solution model is defined by $\dot{\mathbf{p}} = \mathbf{J} \cdot \dot{\mathbf{\Phi}}$, where $\mathbf{J}$ is Jacobian matrix and the joint angles $\mathbf{\Phi} = [\phi_A, \phi_C, \phi_E, \phi_F, \phi_G]^\top$ are the independent control variables. Thus, it is expressed:

$$\dot{\mathbf{p}} = \begin{bmatrix} l_1 c_0 c_s + l_3 c_2 c_s + l_4 c_3 c_s + l_7 c_6 c_s & -l_1 s_6 s_s & -l_3 s_2 s_s & -l_4 s_3 s_s & -l_7 s_6 s_s \\ 0 & l_1 c_0 & l_3 c_2 & l_4 c_3 & l_7 c_6 \\ -l_1 c_0 s_s - l_3 c_2 s_s - l_4 c_3 s_s - l_7 c_6 s_s & -l_1 s_0 c_s & -l_3 s_2 c_s & -l_4 s_3 c_s & -l_7 s_6 c_s \end{bmatrix} \cdot \dot{\mathbf{\Phi}}. \tag{21}$$

Likewise, the inverse algebraic solution is expressed by

$$\dot{\mathbf{\Phi}} = \begin{bmatrix} l_1 c_0 c_s + l_3 c_2 c_s + l_4 c_3 c_s + l_7 c_6 c_s & -l_1 s_6 s_s & -l_3 s_2 s_s & -l_4 s_3 s_s & -l_7 s_6 s_s \\ 0 & l_1 c_0 & l_3 c_2 & l_4 c_3 & l_7 c_6 \\ -l_1 c_0 s_s - l_3 c_2 s_s - l_4 c_3 s_s - l_7 c_6 s_s & -l_1 s_0 c_s & -l_3 s_2 c_s & -l_4 s_3 c_s & -l_7 s_6 c_s \end{bmatrix}^{-1} \cdot \dot{\mathbf{p}}, \tag{22}$$

where the pseudoinverse matrix $\mathbf{J}^+ = (\mathbf{J} \cdot \mathbf{J}^\top)^{-1} \cdot \mathbf{J}$ is an invertible, non singular and non stationary matrix. Moreover, the robots lateral speeds are defined by

$$v_r = \frac{v_5 + v_1}{2} = \quad \frac{\|\dot{\mathbf{q}}_5 + \dot{\mathbf{q}}_1\|}{2}, \quad \text{o} \quad \text{bien} \quad v_l = \|\dot{\mathbf{q}}_4\| \tag{23}$$

and

$$v_l = \frac{v_2 + v_6}{2} = \quad \frac{\|\dot{\mathbf{q}}_2 + \dot{\mathbf{q}}_6\|}{2}, \quad \text{or} \quad v_l = \|\dot{\mathbf{q}}_3\| \tag{24}$$

From Figure 1a, the robot's angular velocity is described by

$$\omega = \frac{2b(v_r - v_l)}{a_t^2 + b_t^2} \tag{25}$$

Considering that a_t and b_t are non constant as legs yaw ϕ_s changes, where $a_t = ||q_5 - q_1||$ and $b_t = |z_r - z_l|$. Moreover, $z_r = E\cos(\phi_s)$ and $z_l = E\cos(\phi_s)$, where E is the instantaneous length from the Klanns rotary point to the end-effectors contact point. When the angle $\phi_s = 0$, then b_t keeps constant and such an angle is aligned to robots longitudinal axis, and producing as a result the following specific case:

$$\omega = \frac{2|z_r - z_l|(\frac{(\|\dot{\mathbf{q}}_5\| + \|\dot{\mathbf{q}}_1\|) - (\|\dot{\mathbf{q}}_2 + \|\dot{\mathbf{q}}_6\|)}{2})}{(\|\mathbf{q}_5\| - \|\mathbf{q}_1\|)^2 + |z_r - z_l|^2} \tag{26}$$

Therefore, the control vector $\dot{\mathbf{u}}$ is algebraically deduced with time-variant control matrix $\mathbf{K}$,

$$\begin{bmatrix} v \\ \omega \end{bmatrix} = \begin{pmatrix} \frac{v_r}{2} + \frac{v_l}{2} \\ \frac{2b}{a_t^2 + b_t^2}(v_r - v_l) \end{pmatrix} = \underbrace{\begin{pmatrix} \frac{1}{2} & \frac{1}{2} \\ \frac{2b}{a_t^2 + b_t^2} & -\frac{2b}{a_t^2 + b_t^2} \end{pmatrix}}_{\mathbf{K}} \cdot \begin{pmatrix} v_r \\ v_l \end{pmatrix} \tag{27}$$

In addition, the functional forms of v_r and v_l are established by the general expression $\lambda \mathbf{q}(\phi_0, \phi_s)^\top$, which is in terms of the robots yaw orientation, such that

$$\begin{pmatrix} v_r \\ v_l \end{pmatrix} = \lambda_{\mathbf{t}} \cdot \begin{pmatrix} \|\dot{\mathbf{q}}_1(\dot{\phi_0}, \dot{\phi_s})\| \\ \vdots \\ \|\dot{\mathbf{q}}_6(\dot{\phi_0}, \dot{\phi_s})\| \end{pmatrix} \tag{28}$$

Where λ is the commutation gait that switches either the right or the left sided tripod, and exchanging the value of the tripod's potential energy P_r or P_l supporting the robots weight $w/3$ at each of the three contact points, defined by

$$\lambda = \begin{cases} \lambda_1, & P_r = hg\sum_i m_i + w/3 \\ \lambda_2, & P_l = hg\sum_i m_i + w/3 \end{cases}$$

The tripod gait commutation is triggered between matrices λ_1 and λ_2 at every time a leg of either tripod completes a cycle, inferred by the coordinate (Gx, Gy) of expression (17). The approach in this work is constrained by two matrices provided as a general model solution that even may be used for up to six actuators (one drive per leg). Each row represents the right-side (row 1) and the left-side (row 2) of the robot's limbs. Each $\lambda_{1,2}$ records the desired user gait, for any matrix element $\lambda_{1,2}(I,j) \neq 0$ establishes a contact point currently stepping ground. If a contact point does physically not match the $\lambda_{1,2}$ in turn, then the drive speed up/down to match it. Hence, the following matrices describe both commuting walking tripods:

$$\lambda_1 = \begin{bmatrix} 1/2 & 0 & 0 & 0 & 1/2 & 0 \\ 0 & 0 & 0 & 1/2 & 0 & 0 \end{bmatrix}, \quad \lambda_2 = \begin{bmatrix} 0 & 0 & 1/2 & 0 & 1/2 & 0 \\ 0 & 1/2 & 0 & 0 & 0 & 0 \end{bmatrix}. \tag{29}$$

Without loss of generality, by commuting both tripods sequentially, Figure 7ab illustrates the limbs Cartesian behaviors along the y component (Figure 5). The hexapod walking tra-

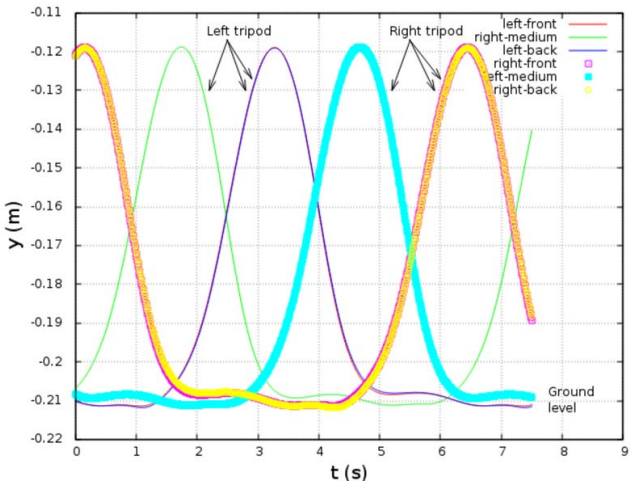

Fig. 5. The six legs tripod walking behavior. Vertical limbs position.

jectory control and the walking reachable spaces with different robot lateral speeds at three different all-limb orientations along forward and backward motions are shown in Figure 6. From the local Cartesian origin, any trajectory depicted below refers to backward navigation. Likewise, any trajectory depicted above the Cartesian origin refers to the robots forward motion. Figure 6 also illustrates when the hexapods lateral speeds are equal, and no angular speed is yielded, each straight trajectory is produced at different all-limb angles at forward and backward motion.

Now, assuming a trajectory reference model to be tracked by the robot, let us define such a reference trajectory vector with two components, both in terms of the first derivative as functions of time,

$$\dot{\mathbf{u}}^{ref} = \begin{pmatrix} v^{ref} \\ \omega^{ref} \end{pmatrix} = \begin{pmatrix} a_0 + a_1 t + a_2 t^2 + ... \\ b_0 + b_1 t + b_2 t^2 + ... \end{pmatrix}, \tag{30}$$

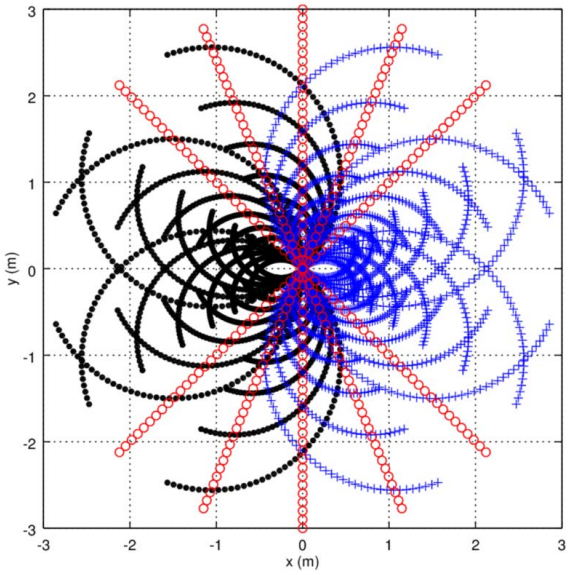

Fig. 6. Robot's mobility nearly full holonomy space, when $v_R > v_L$ (dots), when $v_R < v_L$ (cross), when $v_R = v_L$ (circle) at different θ_t.

where, in the previous reference trajectory model defines the transverse trajectory included in the inverse kinematics control that has been deduced from (30),

$$\boldsymbol{\mu}_{t+1} = \boldsymbol{\mu}_t + \mathbf{K}^{-1} \left(\dot{\mathbf{u}}^{ref} - \hat{\dot{u}}_t \right) \tag{31}$$

From the reference model, the vector of lateral speeds $\dot{\boldsymbol{\mu}} = (v_r, v_l)^\top$ is obtained. Thus, the right-sided tripod is constrained by two legs same speeds $||\dot{\mathbf{p}}_1|| = ||\dot{\mathbf{p}}_5|| = v_r$ and $||\dot{\mathbf{p}}_4|| = v_l$, as well as the left-sided tripod speeds, $||\dot{\mathbf{p}}_2|| = ||\dot{\mathbf{p}}_6|| = v_l$ and $||\dot{\mathbf{p}}_3|| = v_r$. Thus, the contact point Cartesian velocities are

$$\dot{\mathbf{p}}_{1,5} = \frac{v_r^2}{2}, \quad \dot{\mathbf{p}}_4 = v_l^2 \quad \text{and} \quad \dot{\mathbf{p}}_{2,6} = \frac{v_l^2}{2}, \quad \dot{\mathbf{p}}_3 = v_r^2.$$

By using the inverse solution of the Klann kinematics of previous expression (38), the speed contact points are known values, and the linkage vector of angular speeds $\boldsymbol{\Phi} = (\phi_A, \phi_C, \phi_E, \phi_F, \phi_G)^T$ is inferred, and of very particular interest is the Klann s shaft/crank angular speed

$$\dot{\boldsymbol{\Phi}}_{t+1} = \dot{\boldsymbol{\Phi}}_t + \mathbf{J}^{-1} \left(\dot{\mathbf{p}}_t - \mathbf{J} \cdot \dot{\boldsymbol{\Phi}}_t \right) \tag{32}$$

At this point, only $\dot{\phi}_A$ is of interest because represents the angular velocity of the Klann limb's shaft (conducted by a kinematic chain). The three kinematic chain rotary speeds are $\dot{\phi}_{Ar}, \dot{\phi}_{Al}, \dot{\phi}_{As}$, right driving, left driving and steering, respectively. For simplicity, the three rotary variables are represented by the control vector $\dot{\boldsymbol{\Omega}} = (\dot{\phi}_r, \dot{\varphi}_l, \dot{\phi}_s)^\top$. From dynamic equation (51), the following direct dynamic solution for torques $\boldsymbol{\tau} = (\tau_r, \tau_l, \tau_s)^\top$ is deduced,

$$\boldsymbol{\tau} = \begin{pmatrix} r_r \sum_i m_i^r & 0 & 0 \\ 0 & r_l \sum_i m_i^l & 0 \\ 0 & 0 & r_s \sum_i m_i^s \end{pmatrix} \cdot \dot{\boldsymbol{\Omega}}_t \tag{33}$$

Thus, the general main recursive dynamic control equations:

$$\boldsymbol{\tau}_t = \frac{\mathbf{M}}{t_2 - t_1}\left[\mathbf{v}^{ref} - \hat{\mathbf{v}}\right] + \mathbf{C}\left[\mathbf{s}_{t+1} - \mathbf{s}_t\right] \tag{34}$$

And the inverse dynamics that considers the model $\mathbf{v} = r\dot{\boldsymbol{\Omega}}$,

$$\mathbf{v}_{t+1} = \mathbf{v}_t + \mathbf{M}\boldsymbol{\tau}_t\left[t_2 - t_1\right] + \mathbf{M}^{-1}\mathbf{C}\left[\mathbf{s}_{t+1} - \mathbf{s}_t\right] \tag{35}$$

Where v_{t+1} is next desired value at the next control loop. The

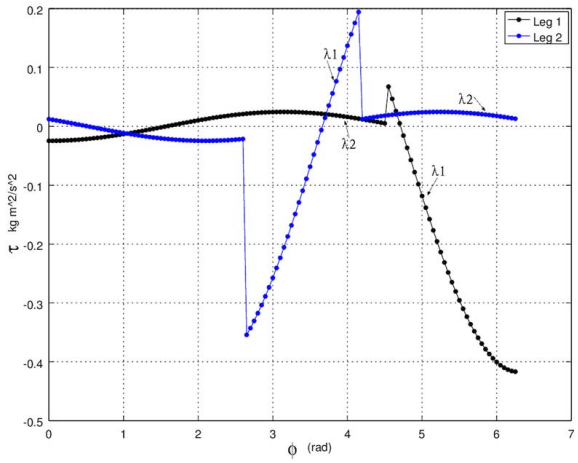

Fig. 7. Cranks torque of right/left legs as tripods switch robot's weight.

robot's total weight is supported by three contact points ($w/3$) during $\pi/2$ of the crank's rotary cycle (Figure 7).

IV. Conclusion

In this work we concluded that as a difference of redundant omnidirectional walking robots capable to move to any direction at any instant of time, with the proposed approach the working space is quasi-omnidirectional as it takes a small latency time to steer the limbs yaw. It is concluded that, despite the Klann mechanism yields planar motion, by including a second DOF for yaw steering, one limbs working space represents a finite subset of the working space of a classical redundant limb, still enough to be used in numerous terrains. In this work, the tripod gait was considered for analysis of hyper-static walking, there are always three contact points on the ground and three on the air synchronously distributed. Nevertheless, in the proposed control law, different types of gaits can easily be implemented just by changing the walking limbs phases and the values of matrices λ_1 and λ_2. In addition, in the proposed kinematic approach, the limbs cycloid shape can be changed varying the lengths of one or more links of the Klann mechanism.

Acknowledgment

The authors thank the Laboratorio de Robótica for technical support to this work. The reported study was funded by the Russian Foundation for Basic Research (RFBR) according to the research project No. *19-58-70002*.

References

[1] HyunGyu, K. DongGyu, L., KyungMin, J., TaeWon S. (2016). Water and Ground-Running Robotic Platform by Repeated Motion of Six Spherical Footpads, IEEE/ASME, Trans. on Mechatronics, vol. 21(1).
[2] Seljanko F. (2012). Thoughts on walking robot for urban search and rescue, IEEE Intl. Conf. on Mechatronics and Autom, 2411-2416.
[3] Horvat T., Karakasiliotis K., Melo K., Fleury L., Thandiackal R., Ijspeert A.J. (2015). Inverse kinematics and reflex based controller for body-limb coordination of a salamander-like robot walking on uneven terrain, IEEE/RSJ Intl. Conf. on Intelligent Robots and Systems, Germany.
[4] Kulandaidaasan J., Mohan R. E., Martnez-Garca E., Tan-Phuc L. (2016). Trajectory Generation and Stability Analysis for Reconfigurable Klann Mechanism Based Walking Robot, Robotics, 5(13), pp. 1-10, MDPI
[5] Kulandaidaasan J., Mohan R. E., Martnez-Garca E., Tan-Phuc L. (2015). Synthesizing reconfigurable foot traces using a Klann mechanism, Robotica, pp. 1-17, Cambridge University Press
[6] El-Farouk E. Labib O., El-Safty S.W., Mueller S., Haalboom T., Strand M. (2018). Towards a Stair Climbing Robot System Based on a Re-configurable Linkage Mechanism, Intell Auton Sys 15. IAS 2018. Adv in Intelli Sys and Comp, vol 867. pp. 278-288, Springer, Cham
[7] Wu J., Yao Y. (2018). Design and analysis of a novel walking vehicle based on leg mechanism with variable topologies, Mechanism and Machine Theory, vol. 128, pp. 663-681, Elsevier
[8] Gilho B.V., Bezerra J. M. (2012). Mechatronic Design of a Chair for Disabled with Locomotion by Legs, ABCM Symposium Series in Mechatronics vol. 5, pp. 1142-1149.
[9] Klann, J.C. (2002). Walking Device. Pat. U.S. 6,478,314 B1, Nov 2002.
[10] Chen X., Wang L., Ye X., Wang G., Wang H. (2013). Prototype development and gait planning of biologically inspired multi-legged crablike robot, Mechatronics 23, 429-444 (2013).
[11] Erden, M.S., Leblebicioglu, K. (2008). Free gait generation with reinforcement learning for a six-legged robot, Auton Syst, 56, 199-212.
[12] Gonzalez de Santos P., Garca E., Estremera J. (2006). Quadrupedal Locomotion: An introduction to the control of four-legged robots, Germany: Springer-Verlag.
[13] Haitao, Y., Haibo, G., Mantian, L., Zongquang, D., Guangjun, L. (2016). Gait generation with smooth transition using CPG-based locomotion control for hexapod walking robot, IEEE Transactions on industrial electronics, (vol.63, no.9, pp.5488-5500), IEEE.
[14] Huang, K., Chen, S., Tsai, M., Liang, F., Hsueh, Y., P-C. Lin, (2012). A Bio-inspired Hexapod Robot with Noncircular Gear Transmission System, IEEE/ASME International Conference on Advanced Intelligent Mechatronics, Kaohsiung, Taiwan: IEEE.
[15] Kazemi, H., Majd, V.J., Moghaddam, M.M. (2013). Modeling and robust backstepping control of an underactuated quadruped robot in bounding motion, Robotica, vol.31, pp.423-439, England: Cambridge Univ Press
[16] Kecskes, I., Burkus, E., Bazso, F., Odry, P. (2015). Model validation of a hexapod walker robot,Robotica, (vol.35, pp.419-462), England: Cambridge Univ Press
[17] Krishna, A., Krishna, N., Pradeep, S., Srihari, K., Sivraj, P. (2014). Design a Fabrication of a Hexapod Robot, International Conference on Embedded Systems, India.
[18] Knoop, E., Conn, A., Rossiter, J. (2017). VAM: Hypocycloid Mechanism for Efficient Bionspired Robotic Gaits, in IEEE Robotics and automation letters, vol.2(2), pp.1055-1061, IEEE.
[19] Martinez-Garcia, E.A., Torres-Mendez, L. A., Mohan, R.E. (2014). Multi-Legged Robot Dynamics Navigation Model with Optical Flow, International Journal of Intelligent Unmanned Systems, vol.2(2), pp.121-139), England, Emerald.
[20] Roennau, A., Heppner, G., Klemm. S., Dillmann, R. (2015). RoaDS-Robot and Dynamics Simulation for Biollogically-Inspired Multi-Legged Walking Robots. IEEE Robotics & Biomimetics, 1870-1876.
[21] Rooney, T., Pearson, M.J., Welsby, J., Horsfield, I., Sewell, R., Dogramadzi, S. (2011). Artificial Active Whiskers for Guiding Underwater Autonomous Walking Robots, CLAWAR 2011, France.
[22] Shekhar, R.S., Khumar P.D. (2011). Dynamic Modeling and Energy Consumption Analysis of Crab Walking of a Six-legged Robot, IEEE Conf. on technologies for Practical Robot Applications. USA, IEEE.
[23] Martínez-García, E.A., (2015). Numerical Modelling in Robotics, (2015)., Spain, OmniaScience, ISBN:978-84-942118-8-1.
[24] Martínez-García, E.A., Uribe, D.R., Mohan, R.E., (2013), Kinematic Manipulability of Multi-Join Bio-Inspired Extremities, J. of Procedia Engineering, vol.64, pp.1533-1542, Elsevier.